Editors' Suggestion

# Kondo interaction of quantum spin Hall edge channels with charge puddles

Christopher Fuchs,[1,2,*] Saquib Shamim,[1,2,3,*] Pragya Shekhar,[1,2,*] Lena Fürst,[1,2] Johannes Kleinlein,[1,2] Jukka I. Väyrynen,[4] Hartmut Buhmann,[1,2] and Laurens W. Molenkamp[1,2]

[1]*Physikalisches Institut (EP3), Universität Würzburg, Am Hubland, 97074 Würzburg, Germany*

[2]*Institute for Topological Insulators, Am Hubland, 97074 Würzburg, Germany*

[3]*Department of Condensed Matter and Material Physics, S. N. Bose National Centre for Basic Sciences, Kolkata 700106, India*

[4]*Department of Physics and Astronomy, Purdue University, West Lafayette, Indiana 47907, USA*

(Received 31 July 2023; accepted 16 October 2023; published 8 November 2023)

Under time-reversal symmetry, quantum spin Hall edge channels are protected against elastic backscattering. However, even for samples which exhibit conductance quantization due to the quantum spin Hall effect, reproducible fluctuations shape the quantization plateau when the chemical potential is tuned through the bulk gap. Here, we examine those fluctuations in micron-sized HgTe quantum well devices. By performing temperature- and gate-dependent measurements, we conclude that "charge puddles" in the narrow-gap material have a Kondo-type interaction with the edge channels resulting in the observed conductance fluctuations. Our results provide insight into the underlying mechanisms of scattering in quantum spin Hall edge channels.

DOI: 10.1103/PhysRevB.108.205302

## I. INTRODUCTION

After the first experimental observation of the quantum spin Hall effect in HgTe quantum wells, the robustness of the conductance quantization in the presence of impurities has been vigorously investigated. Although theory predicts that the helical edge channels are protected against elastic backscattering under time-reversal symmetry, all experimental demonstrations of the quantum spin Hall effect, including the first report in 2007, show gate voltage-dependent reproducible fluctuations in the quantum spin Hall conductance [1–4]. These fluctuations have been attributed to inelastic scattering off of charge puddles, which are common in narrow-gap semiconductors and are formed due to an inhomogeneous potential landscape [2,5–8]. In Ref. [7], Väyrynen *et al.* consider interactions of helical edge channels with charge puddles small enough to show single electron charging effects: changing the gate voltage leads to charging of the puddle in single electron steps, which results in fluctuations in the quantum spin Hall conductance due to resonant backscattering. They further predict that Kondo effects in the puddle (depending on odd or even occupancy) lead to a distinct temperature dependence of these conductance fluctuations.

We recently have been able to demonstrate Kondo effects on topological edge channels in magnetically doped (Hg,Mn)Te quantum wells [9], which exhibit Kondo temperatures up to ∼3 K. However, for the Kondo effects of charge puddles one expects a much lower Kondo temperature (plausibly $\lesssim$ 100 mK, as explained later) and up until now, it has not been possible to verify the above predictions because conventional dry etching, routinely used to fabricate HgTe-based quantum spin Hall microstructures, causes significant damage to the edges and consequently creates a large number of scatterers in these devices [3,5,10], making mechanistic studies problematic. We recently showed that a wet-etch fabrication process results in high-quality microstructures with mobilities similar to macroscopic devices [3]. In this paper, we investigate the conductance fluctuations of quantum spin Hall edge channels at different temperatures between 20 mK and 2 K in micron-sized devices fabricated from HgTe quantum wells using the wet-etch process. The fluctuations in conductance in the regime of edge channel transport exhibit a characteristic temperature dependence which can be related to interactions of the helical edge channels with a charge puddle acting as a Kondo-correlated quantum dot.

## II. MATERIAL GROWTH AND DEVICE FABRICATION

We use molecular beam epitaxy to grow a 7.5-nm-thick HgTe quantum well sandwiched between (Hg,Cd)Te barriers on a lattice-matched (Cd,Zn)Te substrate. A schematic of the corresponding layer stack is shown in the inset of Fig. 1(b). For a carrier density of $n \sim 6 \times 10^{11}$ cm$^{-2}$, the mobility is $\mu \sim 2 \times 10^5$ cm$^2$ V$^{-1}$ s$^{-1}$ (which corresponds to a mean free path of $l \sim 2.5$ μm). We fabricated a four-terminal (Device 1) and a three-terminal (Device 2) device as shown in the schematic of Figs. 1(a) and 1(b), respectively, using e-beam lithography and chemical wet etching. Details of the device fabrication can be found in Refs. [3,11]. All electrical transport measurements are performed in dilution refrigerators using low-frequency (∼13 Hz) lock-in techniques.

## III. FLUCTUATIONS OF THE QUANTUM SPIN HALL CONDUCTANCE IN MICRON-SIZED DEVICE

The gate-voltage characteristics of Device 1 and Device 2 are shown in Figs. 1(a) and 1(b), respectively. A gate electrode can be used to tune the carrier density from *n*-type to *p*-type conductance which ensures that the entire regime of

*These authors contributed equally to this work.

 

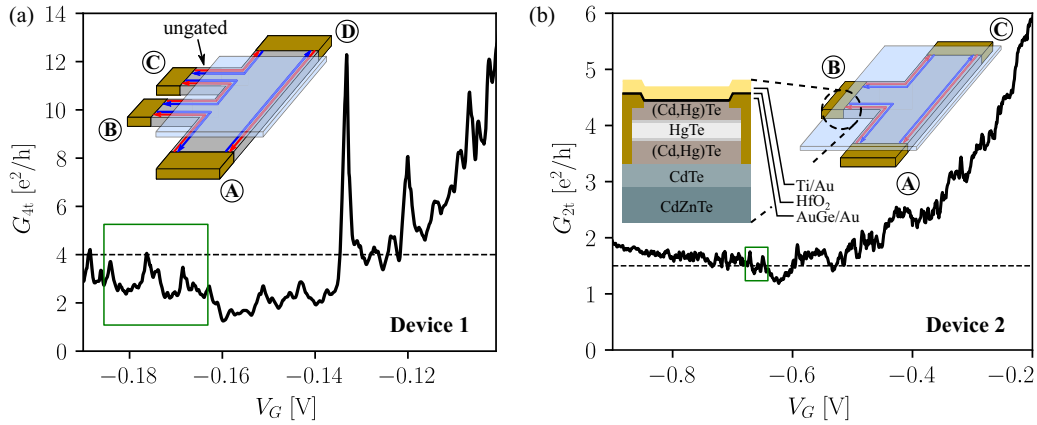


FIG. 1. Conductance fluctuations in the quantum spin Hall regime. (a) The four-terminal conductance $G_{4t} = I_{A,D}/V_{B,C}$ of Device 1 is plotted as a function of gate voltage $V_G$ at 17 mK. The dashed line indicates the expected quantization conductance ($4\,e^2/h$) for a four-terminal device. The inset shows a schematic of the device. The letters $A$, $B$, $C$, and $D$ indicate Ohmic contacts. The distance between the contacts $B$ and $C$ is ∼1.7 μm. (b) The two-terminal conductance $G_{2t} = I_{A,C}/V_{A,C}$ of Device 2 is plotted as a function of $V_G$ at 27 mK. The dashed line indicates the expected quantization conductance ($3/2\,e^2/h$) for a three-terminal device. The inset shows a schematic of the device along with the molecular beam epitaxy grown layer stack. The distance between the contacts $A$ and $C$ is ∼3 μm. The width is ∼2 μm for both devices. The CdTe, (Hg,Cd)Te bottom and top barriers have a thickness of 50, 150, and 15 nm, respectively. The green boxes indicate the regions of interest for the study of fluctuations in these devices.

topological edge channel transport is accessible. Since Device 2 employs a thick dielectric layer (85-nm-thick $HfO_2$) compared to Device 1 (14-nm-thick $HfO_2$), the gate efficiency of Device 1 is larger than in Device 2. When the chemical potential is tuned through the bulk band gap, the conductance shows a minimum for both devices, which corresponds to the quantum spin Hall regime. While for Device 2, the conductance is close to the value expected from the Landauer-Büttiker model [denoted by dashed lines in Figs. 1(a) and 1(b)] for the given measurement geometry, for Device 1, the conductance is lower than the expected value by 50%. Such deviation in conductance from the expected quantized value has been observed before and has been attributed to scattering from charge puddles [5]. Even though the conductance is close to quantization, we observe fluctuations in the quantum spin Hall conductance for both devices. These conductance fluctuations are reproducible for various gate sweeps at a fixed temperature. Even though the absolute magnitudes of the conductance fluctuations are different in Device 1 and Device 2 (see Fig. 1), the relative conductance fluctuations $\Delta G/G$ and the temperature dependence of the fluctuations are similar for both devices, as elaborated in the following.

## IV. TEMPERATURE DEPENDENCE OF THE CONDUCTANCE FLUCTUATIONS

A very distinct temperature dependence of the conductance fluctuations is observed for the gate-voltage regions indicated by the green boxes (see Fig. 1), which is displayed in Figs. 2(a) and 2(b) for Device 1 and Device 2, respectively. The temperature dependence of the conductance in extended gate-voltage regions is shown in Figs. 1 and 2 of the Supplemental Material [12], along with similar observations in an additional device. As shown in Fig. 2, the amplitude of the conductance fluctuations increases monotonically as the temperature decreases. In the high-temperature limit (red curve), the conductance traces exhibit alternating conductance peaks and valleys, which are indicated by vertical lines. In the temperature evolution of the peaks, we observe the following main features: the conductance value at peaks labeled as $P_{ev}$—referred to as even peaks for reasons that will become obvious below—remains essentially constant for all temperatures. However, for the neighboring peaks labeled as $P_{odd}$—referred to as odd peaks—the conductance decreases with decreasing temperature. To quantify the difference between odd and even peaks, the temperature-dependent change in conductance $\Delta G(T) = G(T) - G(T \approx 2\ \mathrm{K})$ is shown in Figs. 3(a) and 3(b) for Device 1 and Device 2, respectively. In contrast, the conductance at all valleys shows a similar temperature dependence: $\Delta G(T)$ decreases with decreasing temperature [right panels in Figs. 3(a) and 3(b)]. The distinct temperature dependence of the conductance fluctuations at odd and even peaks evidently is strongly reminiscent of the conductance $G_{QD}$ of a Kondo-correlated quantum dot, that alternates between even and odd electron occupancy as the gate voltage is varied [13,14]. Hence the peak labeling we have chosen.

## V. INTERACTIONS BETWEEN HELICAL EDGE CHANNELS AND A CHARGE PUDDLE ACTING AS A KONDO-CORRELATED QUANTUM DOT

To qualitatively explain various features of the conductance versus gate-voltage traces at different temperatures, we assume that a charge puddle, acting as a quantum dot, is in close proximity to the helical edge channels, thus allowing for significant wave function overlap [Fig. 4(a)]. When the gate voltage is used to tune the electrochemical potential, we simultaneously change the potential for the edge channels as well as for the dot, which leads to Coulomb oscillations of the edge-dot transmission amplitude (and conductance) [Fig. 4(b)].

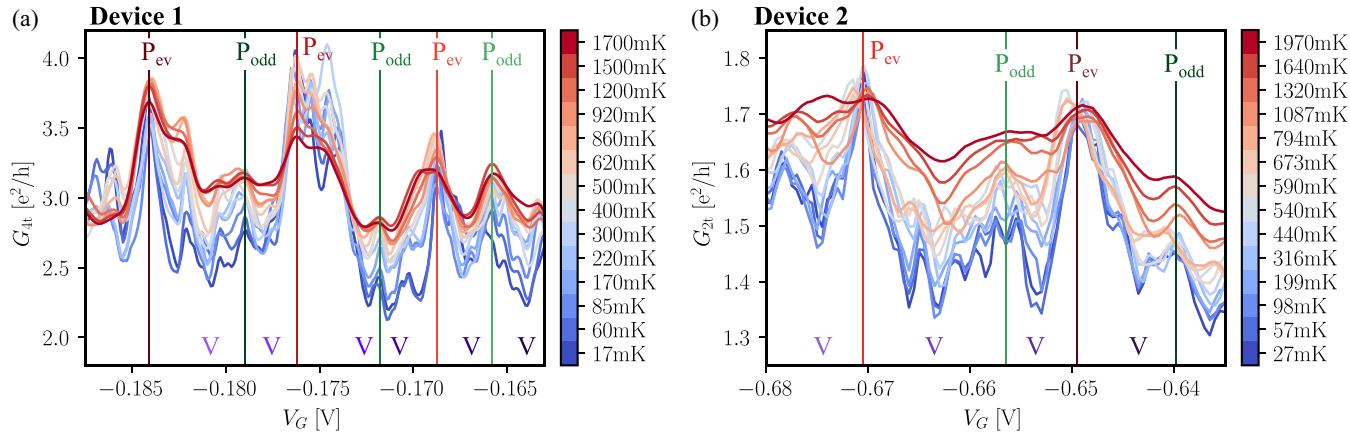


FIG. 2. Odd-even patterns in the temperature dependence of the conductance fluctuations. (a) $G_{4t}$ as a function of $V_G$ from 17 mK (blue) to 1.7 K (red) for Device 1. (b) $G_{2t}$ as a function of $V_G$ from 27 mK (blue) to 2 K (red) for Device 2. The various conductance peaks are labeled as $P_{ev}$ and $P_{odd}$ (indicated by vertical lines) while the valleys are labeled as $V$.

Figures 4(b) and 4(c) show schematically the temperature dependence of the conductance of a quantum dot and quantum spin Hall edge channels interacting with a dot, respectively. For $T > T_K$ and at gate voltages where the dot is Coulomb blockaded (i.e., $T < E_c$, the charging energy of the dot), any interactions of the dot with electrons outside are cut off. In this situation, the conductance of the helical edge channels remains close to the expected quantized value. For gate voltages where the edge-dot transmission is high, the dot can interact with the carriers in the helical edge channels. Spin-flip scattering of edge channel electrons with those on the dot [7] results in backscattering, leading to a decrease in channel conductance. Thus, valleys (peaks) in the conductance of the edge-dot connection correspond to peaks (valleys) in the quantum spin Hall conductance. On lowering the temperature, the reduced thermal smearing causes the conductance of the edge-dot junction to increase for all peaks, hence bringing about a decrease in the quantum spin Hall conductance for all valleys. For $T \sim T_K$, the edge-dot transmission in odd valleys (occupancy with an odd number of electrons, resulting in a net spin) increases strongly due to the Kondo effect [13,14]. The dot now can interact with edge channel electrons for all gate voltages where the dot occupation number is odd, resulting in backscattering and hence a decrease in the quantum spin Hall conductance for odd peaks. Thus, odd peaks in the quantum spin Hall conductance show a strong temperature dependence. For an even occupancy the dot remains blockaded at low temperatures, hence even peaks in the quantum spin Hall conductance show a weak temperature dependence, remaining close to the quantized value. This model qualitatively reproduces the features of conductance versus gate-voltage curves at different temperatures shown in Fig. 2.

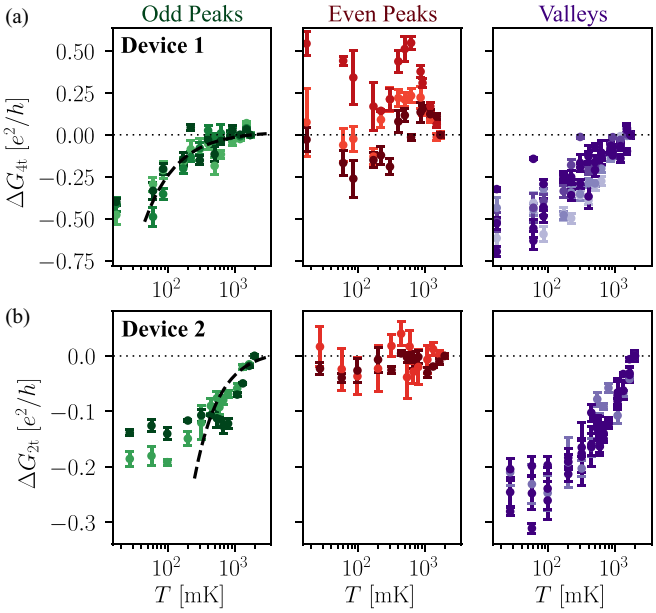


FIG. 3. Temperature evolution of odd and even peaks. The temperature-dependent change in conductance $\Delta G(T) = G(T) - G(T_{High})$ of the peaks marked in Fig. 2 for (a) Device 1 ($T_{High} = 1.7$ K) and (b) Device 2 ($T_{High} = 2.0$ K). The color code corresponds to the color map of the labels for $P$ and $V$ introduced in Fig. 2. The dashed lines indicate fits to Eq. (1). In Device 2, the temperature dependence saturates at ~200 mK, which we attribute to higher electron temperature during the measurement compared to Device 1 (~50 mK). The error bars are based on a maximum error estimation in 0.2 mV (Device 1) and 0.6 mV (Device 2) windows around the vertical lines in Fig. 2.

The voltage spacing between neighboring peaks $V_{pp}$, about 4 mV for Device 1 and 10 mV for Device 2 (see Fig. 2), implies a charging energy of 2 and 5 meV, respectively. The Coulomb blockade requirement $E_C > T$ is thus obeyed for both devices. A simple capacitor model reveals charge puddle diameters of approximately 100 nm for both devices. Details of these calculations are given in the Supplemental Material [12].

Additional charge puddles, further away from the edge channels and weaker in interactions, may give rise to further conductance features that arise in the low-temperature limit, (cf. Fig. 2). The applied gate voltage tunes the chemical potential through all band edge and puddle states simultaneously, all with their own energetic substructure, which slightly modulates the observed periodicity of peaks and valleys. In extended gate-voltage regions (that are shown in the Supplemental Material [12]) more charge puddles will be able to

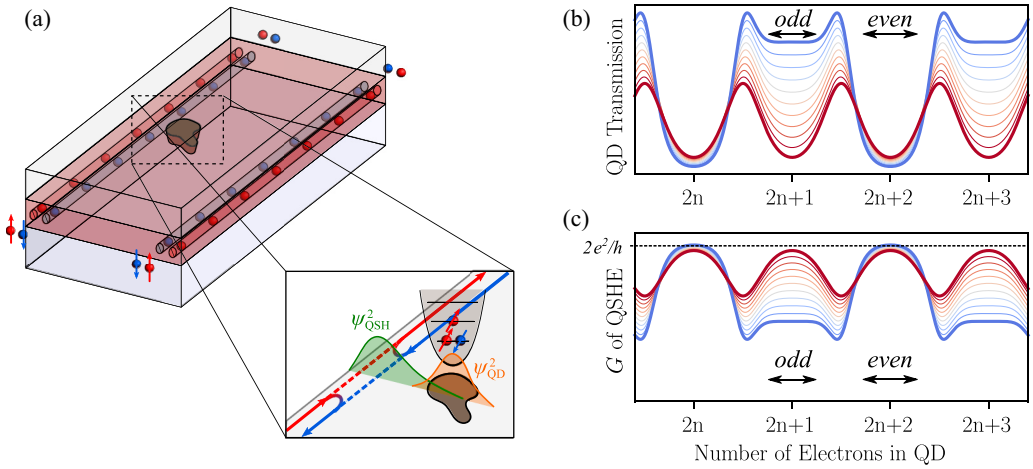


FIG. 4. Fluctuations based on the interaction between edge channels and a charge puddle. (a) A schematic of the helical edge channels and the Kondo quantum dot formed by a charge puddle in the vicinity of the edge channels. The inset indicates the wave function overlap of edge channels and quantum dot states. The out-of-plane arrows indicate the orientation of the spin eigenstates of helical edge electrons (spin momentum locked) and the quantum dot system which are not necessarily parallel to each other, as further discussed in the Appendix. (b) Temperature dependence of the conductance of a Kondo-correlated quantum dot as a function of occupation number, where red indicates high ($T > T_K$) and blue low ($T \sim T_K$) temperatures. (c) An illustration of the corresponding quantum spin Hall conductance due to the interaction between helical edge channels and a Kondo quantum dot as described in the main text.

interact with the edge channel, leading to an averaging out of the odd-even signal in the conductance trace. Thus, the odd-even effect is observed only if the sample is in the quantum spin Hall transport regime and a charge puddle (that is in the Coulomb blockade regime and overlaps the edge channels) is charged/depleted simultaneously. This limits the observation to (a) a high-quality sample with only few charge puddles as well as (b) a limited voltage range where a single dominant charge puddle fulfills the backscattering requirements.

A comparison of our observations with the predictions of Ref. [7] reveals a major difference: while we observe that the quantum spin Hall conductance *decreases* away from the expected quantized value with decreasing temperature, Ref. [7] predicts that the conductance *increases* monotonically with decreasing temperature. This is because of the exchange mechanism that is being considered in [7]. Kondo scattering of helical edge channels has previously been investigated by multiple works, starting with the study by Maciejko *et al.* based on "isotropic" exchange, i.e., terms that conserve the $z$ component of the total spin in the exchange Hamiltonian ($z$ is the helical edge quantization axis), between edge channel carriers and magnetic impurities in vicinity to the edge [15]. The theory described in the paper tacitly assumes the spin of the magnetic impurities is allowed to relax, leading to a nonzero net backscattering rate. In a later paper [16], Tanaka *et al.* show that in a strictly spin-conserving system the backscattering rate vanishes in the dc limit. In such a picture, that assumes zero spin relaxation, only "anisotropic" (spin-$z$-nonconserving) exchange would lead to a net deviation of the edge channel conductance in the according model. Later works (e.g., [7,17]) use such higher order anisotropic exchange models to describe the Kondo interaction between the edge channels and magnetic impurities, such as quantum dots. In Ref. [7], anisotropic exchange scattering arises from the breaking of spin-rotation symmetry within the dot, while Ref. [17] shows that the effect can also arise from symmetry breaking on the edge.

However, we have recently shown experimentally that isotropic Kondo interactions actually do describe scattering with paramagnetic impurities in (Hg,Mn)Te quantum wells [9], clearly indicating that the modeling of Ref. [15] is appropriate for our material system. At the same time, this implies that the impurity spin should be allowed to relax when modeling Kondo interactions in HgTe. We show below theoretically that by including the possibility of spin relaxation of the Kondo quantum dot, implicit in the qualitative model we discussed above, the isotropic exchange model does become consistent with our experimental observations.

To calculate the expected temperature-dependent corrections to the quantized conductance due to isotropic exchange scattering and spin relaxation, we assume that the spin of an edge channel electron $\mathbf{s}$ is coupled to a magnetic impurity which models the spin of the dot $\mathbf{S}$. The corresponding Kondo Hamiltonian takes the form $H_{\mathrm{K}} = J_0 \mathbf{s} \cdot \mathbf{S}$ where $J_0$ is the exchange coupling. This Hamiltonian leads to a Korringa spin-flip rate $\tau_K^{-1} = \pi T (\rho J_0)^2 f(T)$ of the dot spin due to its coupling to the helical edge state. Here $f(T)$ is a temperature-dependent factor that accounts for Kondo and/or Luttinger liquid renormalizations. At low temperature (but above the bias voltage, $eV \ll k_B T$), we have $f(T) \propto T^{2(1-K)}$, where $K$ is the Luttinger liquid interaction parameter. Crucially, $1/\tau_K$ also determines the rate of backscattering of the edge electrons. However, since $H_K$ conserves the total spin projection along the $z$ axis $s_z + S_z$, it alone would not give rise to a conductance correction [7,16] as both left- and right-moving electrons would be backscattered at equal rates. This balance will be broken when the spin $\mathbf{S}$ has an independent relaxation channel. Denoting the corresponding relaxation rate $\tau_{\mathrm{bath}}^{-1}$, we show that the correction to the helical edge current is $\delta I \propto \frac{eV}{k_B T (\tau_K + \tau_{\mathrm{bath}})}$.

When the spin relaxation of the magnetic impurity is faster than consecutive backscattering events ($\tau_{\text{bath}} \ll \tau_K$), the correction to the quantized conductance $\Delta G$ is fully determined by the spin-flip rate due to isotropic exchange interaction,

$$\Delta G = \frac{e^2}{4k_B T \tau_K} \propto T^{-2(1-K)}. \tag{1}$$

The details of the calculation can be found in the Appendix. Following Refs. [9,18], and using the applicable device parameters, we calculate $K \sim 0.55$ and 0.41 for Device 1 and Device 2, respectively. Using these values for $K$, we fit the experimental data in the left panels of Fig. 3 to Eq. (1) (dashed curves are the fit). The fitting parameters are the amplitude and a constant offset (which corrects that $T \sim 2$ K is only estimating the high-temperature limit). The theoretical curve matches the experimental data well for Device 1. Plotting the data of Device 1 in a double logarithmic scale (see [12]) further indicates that the temperature dependence is indeed described by the power law of Eq. (1). This confirms that the observed temperature-dependent correction to the quantum spin Hall conductance can indeed be described by isotropic exchange interactions with a charge puddle acting as a few electron quantum dot that exhibits Kondo effects. For Device 2 the model also reproduces the general trend of $\Delta G$, though the fit is not as good as for Device 1. We attribute this to the elevated base electron temperature during the experiment on Device 2 (a saturation below ∼200 mK can be seen in Fig. 3(b), while Fig. 3(a) only saturates below ∼50 mK). This difference is because two different dilution refrigerators have been used for the two devices.

Within the scope of this work, the microscopic origin of the relaxation channel giving rise to $\tau_{\text{bath}}$ cannot be exactly identified, but a list of candidates includes spin exchange via (1) hyperfine interactions (contact hyperfine [19,20] or mean-field [21]), (2) interactions with a network of (bulk) charge puddles [5,10], or (3) interactions with $Hg^+$ acceptorlike vacancies [22]. Out of the list of candidates, direct-exchange contact hyperfine interaction seems most plausible because of the strong contribution from 6*s* electrons of Hg to the electronic wave function of HgTe. Future investigation is needed to understand the spin relaxation in detail.

## VI. DISCUSSION

In a recent work, we showed that the isotropic Kondo effect, discussed by Maciejko *et al.* [15], appropriately describes scattering of helical edge electrons with paramagnetic Mn dopants in (Hg,Mn)Te quantum wells [9]. Both Ref. [9] and the present work describe scattering of quantum spin Hall edge channels at impurity states due to the same underlying mechanism, which is the isotropic Kondo effect. The two experiments deviate from each other in representing the two opposite Kondo limits that were presented in Ref. [15]: Below the Kondo temperature—which is around 3 K for the strongly paramagnetic Mn dopants—quantized conductance is observed in the very low-temperature Kondo limit, as the Kondo effect there becomes suppressed by Kondo shielding (Kondo cloud) [9]. The high-temperature Kondo limit could not be accessed in Ref. [9], because of thermal carrier excitation at temperatures above ∼10 K. In contrast, in the present work, we observe no signs of saturation of the Kondo effect at low temperatures before the electron temperature limit is reached [see Fig. 2(a)]. We attribute the small Kondo temperature, significantly below 100 mK, to the weaker interaction between edge channels and charge puddles. The conductance approaches quantized conductance in the high-temperature limit. The range of temperatures that we investigated is similar for both Ref. [9] and this work, as this is the temperature range in which narrow-gap semiconductors can be probed without significant thermal excitations above the bulk gap. Combining the findings of Ref. [9] and this work, the experimental evidence of both temperature limits of the isotropic Kondo exchange mechanism indicates that the early work by Maciejko *et al.* [15] reliably describes Kondo-based backscattering mechanisms of quantum spin Hall edge channels over a broad temperature range.

Almost 15 years after the first observation of the quantum spin Hall effect, this work finally provides experimental insights into the mechanism that causes gate voltage-dependent fluctuations in otherwise quantized samples. Charge puddles are identified as the dominant source of backscattering in the helical edge channels. The microscopic mechanism of backscattering involves an isotropic exchange between the helical edge channels and charge puddles acting as Kondo quantum dots with spin relaxation. Puddles are present in any narrow-gap material, and it is very likely similar mechanisms as shown here are at play in other two-dimensional topological materials. This study lays the groundwork for further efforts to reduce backscattering in quantum spin Hall devices leading to more efficient applications in spintronics.

## ACKNOWLEDGMENTS

The work in Würzburg was supported by the Deutsche Forschungsgemeinschaft (DFG, German Research Foundation) in the project SFB 1170 (Project ID 258499086) and in the Würzburg-Dresden Cluster of Excellence on Complexity and Topology in Quantum Matter *ct.qmat* (EXC 2147, Project ID 390858490), and by the Free State of Bavaria (Institute for Topological Insulators). Theoretical work of J.I.V. was supported by the U.S. Department of Energy, Office of Science, National Quantum Information Science Research Centers, Quantum Science Center.

## APPENDIX: HELICAL EDGE COUPLED TO A MAGNETIC IMPURITY WITH A RELAXATION CHANNEL

We consider a helical edge (spin $\mathbf{s}$) isotropically coupled to a magnetic impurity $\mathbf{S}$ at some position $x_0$ along the edge. The corresponding exchange interaction Hamiltonian is

$$H_{\text{K}} = J_0 \mathbf{s}(x_0) \cdot \mathbf{S}. \tag{A1}$$

Additionally, we assume that the impurity spin $\mathbf{S}$ is coupled to an additional relaxation channel, such as due to an environmental spin bath. We trace out the environment, giving rise to a decay of $\mathbf{S}$ with a rate $\tau_{\text{bath}}^{-1}$ [see Eq. (A3) below].

We can write the backscattering current operator $\delta I$ as the rate of change of the difference between the number of right and left movers on the edge, $\delta I = -ed(\delta N)/dt$ where

$\delta N = (N_R - N_L)/2$ [23]. On the helical edge, the operator $\delta N$ is related to the $z$ component of the total helical electron spin, $\delta N = \hbar^{-1}\int dx\, s_z(x)$. The Hamiltonian $H_{\rm K}$ conserves the $z$ component of the total spin of the combined edge-impurity system, $[H_{\rm K}, \hbar\delta N + S_z] = 0$. For a magnetic impurity formed by a quantum dot, any spin projection is generally not conserved. Nevertheless, one can choose a basis where the spin projection at the tunneling point is quantized along the $z$ axis [7], which is what we have done here.

We take advantage of the conservation law by noting that $d\langle S_z\rangle/dt$ vanishes in the steady state [7]. Thus, we can add this term to $\langle \delta I\rangle$ so that

$$\langle \delta I\rangle = -e\frac{d}{dt}\langle \delta N + \hbar^{-1}S_z\rangle. \tag{A2}$$

For $d\langle S_z\rangle/dt$, we include the unitary time evolution due to $H_{\rm K}$ and the nonunitary time evolution that models the spin relaxation due to an environment,

$$\frac{d}{dt}\langle S_z\rangle = \frac{i}{\hbar}\langle [H_{\rm K}, S_z]\rangle - \tau_{\rm bath}^{-1}\langle S_z\rangle. \tag{A3}$$

The unitary piece cancels out due to the aforementioned conservation law [16], so that

$$\langle \delta I\rangle = e\tau_{\rm bath}^{-1}\langle S_z\rangle/\hbar. \tag{A4}$$

We are now left with the task of evaluating the steady-state spin polarization $\langle S_z\rangle$. For this, we use the Bloch equation, which is obtained by tracing out both the spin bath as well as the itinerant electrons of the helical edge [7,23]. We find

$$\frac{d}{dt}\langle S_z(t)\rangle = -\tau_K^{-1}\left[\langle S_z(t)\rangle - S_z^f\right] - \tau_{\rm bath}^{-1}\langle S_z(t)\rangle. \tag{A5}$$

Here $\tau_K^{-1} = \pi T(\rho J_0)^2 f(T,V)$ is the Korringa spin-flip rate [24] due to the coupling to the helical edge (density of states $\rho$). The function $f$ contains the renormalization of the exchange coupling,

$$f(T,V) = K^2\left(\frac{v/a}{2\pi k_B T}\right)^{2-2K} B\left(K + i\frac{eV}{2\pi k_B T}, K - i\frac{eV}{2\pi k_B T}\right) \times \cosh\left(\frac{eV}{2k_B T}\right), \tag{A6}$$

and $K < 1$ is the Luttinger liquid parameter repulsive interactions, $a$ is the short-distance cutoff, $v$ is the helical edge velocity, and $B$ is the beta function.

In the Bloch equation (A5), $S_z^f = (\hbar/2)\tanh(eV/2k_BT)$ would be the steady-state polarization of the magnetic impurity if there we no spin relaxation due to the spin bath. The polarization is caused by the coupling to the helical edge which obtains a magnetization $\langle s_z\rangle \propto eV$ when a bias voltage $V$ is applied. The additional spin-relaxation channel (relaxation rate $\tau_{\rm bath}^{-1}$) due to, e.g., a spin bath will lead to a somewhat smaller steady-state spin polarization,

$$\langle S_z\rangle = \frac{\hbar}{2}\frac{\tau_K^{-1}}{\tau_K^{-1} + \tau_{\rm bath}^{-1}}\tanh\frac{eV}{2k_BT}, \tag{A7}$$

obtained by solving $\frac{d}{dt}\langle S_z(t)\rangle = 0$ in Eq. (A5). Using the steady state $\langle S_z\rangle$ in Eq. (A4) yields the steady-state backscattering current,

$$\langle \delta I\rangle = e\frac{1}{2}\frac{\tau_{\rm bath}^{-1}\tau_K^{-1}}{\tau_K^{-1} + \tau_{\rm bath}^{-1}}\tanh\frac{eV}{2k_BT}. \tag{A8}$$

The linear response limit $eV \ll k_BT$ was used in the main text. The prefactor $\langle \delta I\rangle$ has a simple interpretation: it takes a total time $\tau_K + \tau_{\rm bath}$ for a helical edge electron to backscatter ($\tau_K$ to backscatter and then $\tau_{\rm bath}$ for the impurity spin to "reset," allowing the next electron to backscatter).


[1] M. König, S. Wiedmann, C. Brüne, A. Roth, H. Buhmann, L. W. Molenkamp, X. Qi, and S. Zhang, Quantum spin Hall insulator state in HgTe quantum wells, Science **318**, 766 (2007).

[2] A. Roth, C. Brüne, H. Buhmann, L. W. Molenkamp, J. Maciejko, X. Qi, and S. Zhang, Nonlocal transport in the quantum spin Hall state, Science **325**, 294 (2009).

[3] K. Bendias, S. Shamim, O. Herrmann, A. Budewitz, P. Shekhar, P. Leubner, J. Kleinlein, E. Bocquillon, H. Buhmann, and L. W. Molenkamp, High mobility HgTe microstructures for quantum spin Hall studies, Nano Lett. **18**, 4831 (2018).

[4] S. Wu, V. Fatemi, Q. D. Gibson, K. Watanabe, T. Taniguchi, R. J. Cava, and P. Jarillo-Herrero, Observation of the quantum spin Hall effect up to 100 kelvin in a monolayer crystal, Science **359**, 76 (2018).

[5] L. Lunczer, P. Leubner, M. Endres, V. L. Müller, C. Brüne, H. Buhmann, and L. W. Molenkamp, Approaching quantization in macroscopic quantum spin Hall devices through gate training, Phys. Rev. Lett. **123**, 047701 (2019).

[6] J. I. Väyrynen, M. Goldstein, and L. I. Glazman, Helical edge resistance introduced by charge puddles, Phys. Rev. Lett. **110**, 216402 (2013).

[7] J. I. Väyrynen, M. Goldstein, Y. Gefen, and L. I. Glazman, Resistance of helical edges formed in a semiconductor heterostructure, Phys. Rev. B **90**, 115309 (2014).

[8] A. Gourmelon, E. Frigerio, H. Kamata, L. Lunczer, A. Denis, P. Morfin, M. Rosticher, J.-M. Berroir, G. Fève, B. Plaçais, H. Buhmann, L. W. Molenkamp, and E. Bocquillon, Velocity and confinement of edge plasmons in HgTe-based two-dimensional topological insulators, Phys. Rev. B **108**, 035405 (2023).

[9] S. Shamim, W. Beugeling, P. Shekhar, K. Bendias, L. Lunczer, J. Kleinlein, H. Buhmann, and L. W. Molenkamp, Quantized spin Hall conductance in a magnetically doped two dimensional topological insulator, Nat. Commun. **12**, 3193 (2021).

[10] S. Shamim, P. Shekhar, W. Beugeling, J. Böttcher, A. Budewitz, J.-B. Mayer, L. Lunczer, E. M. Hankiewicz, H. Buhmann, and L. W. Molenkamp, Counterpropagating topological and quantum Hall edge channels, Nat. Commun. **13**, 2682 (2022).

[11] P. Shekhar, S. Shamim, S. Hartinger, R. Schlereth, V. Hock, H. Buhmann, J. Kleinlein, and L. W. Molenkamp, Low-temperature atomic layer deposition of hafnium oxide for gating applications, ACS Appl. Mater. Interfaces **14**, 33960 (2022).

[12] See Supplemental Material at http://link.aps.org/supplemental/10.1103/PhysRevB.108.205302 for extended data, supporting figures, and an estimation of the quantum dot size.

[13] D. Goldhaber-Gordon, H. Shtrikman, D. Mahalu, D. Abusch-Magder, U. Meirav, and M. A. Kastner, Kondo effect in a single-electron transistor, Nature (London) **391**, 156 (1998).

[14] W. G. van der Wiel, S. D. Franceschi, T. Fujisawa, J. M. Elzerman, S. Tarucha, and L. P. Kouwenhoven, The Kondo effect in the unitary limit, Science **289**, 2105 (2000).

[15] J. Maciejko, C. Liu, Y. Oreg, X.-L. Qi, C. Wu, and S.-C. Zhang, Kondo effect in the helical edge liquid of the quantum spin Hall state, Phys. Rev. Lett. **102**, 256803 (2009).

[16] Y. Tanaka, A. Furusaki, and K. A. Matveev, Conductance of a helical edge liquid coupled to a magnetic impurity, Phys. Rev. Lett. **106**, 236402 (2011).

[17] O. M. Yevtushenko and V. I. Yudson, Suppression of ballistic helical transport by isotropic dynamical magnetic impurities, Phys. Rev. B **104**, 195414 (2021).

[18] J. C. Y. Teo and C. L. Kane, Critical behavior of a point contact in a quantum spin Hall insulator, Phys. Rev. B **79**, 235321 (2009).

[19] B. E. Kane, A silicon-based nuclear spin quantum computer, Nature (London) **393**, 133 (1998).

[20] F. A. Zwanenburg, A. S. Dzurak, A. Morello, M. Y. Simmons, L. C. L. Hollenberg, G. Klimeck, S. Rogge, S. N. Coppersmith, and M. A. Eriksson, Silicon quantum electronics, Rev. Mod. Phys. **85**, 961 (2013).

[21] A. M. Lunde and G. Platero, Hyperfine interactions in two-dimensional HgTe topological insulators, Phys. Rev. B **88**, 115411 (2013).

[22] T. Dietl, Effects of charge dopants in quantum spin Hall materials, Phys. Rev. Lett. **130**, 086202 (2023).

[23] J. I. Väyrynen and L. I. Glazman, Current noise from a magnetic moment in a helical edge, Phys. Rev. Lett. **118**, 106802 (2017).

[24] J. Korringa, Nuclear magnetic relaxation and resonance line shift in metals, Physica **16**, 601 (1950).